Efficient synthesis of phycocyanobilin in mammalian cells for optogenetic control of cell signaling

Youichi Uda[a,b,c], Yuhei Goto[b,c], Shigekazu Oda[b,c], Takayuki Kohchi[d], Michiyuki Matsuda[a,e], and Kazuhiro Aoki[b,c,f,g,1]

[a]Department of Pathology and Biology of Diseases, Graduate School of Medicine, Kyoto University, Kyoto 606-8501, Japan; [b]Okazaki Institute for Integrative Bioscience, National Institutes of Natural Sciences, Okazaki, Aichi 444-8787, Japan; [c]Division of Quantitative Biology, National Institute for Basic Biology, National Institutes of Natural Sciences, Okazaki, Aichi 444-8787, Japan; [d]Laboratory of Plant Molecular Biology, Graduate School of Biostudies, Kyoto University, Kyoto 606-8502, Japan; [e]Laboratory of Bioimaging and Cell Signaling, Graduate School of Biostudies, Kyoto University, Kyoto 606-8501, Japan; [f]Imaging Platform for Spatio-Temporal Information, Graduate School of Medicine, Kyoto University, Kyoto 606-8501, Japan; and [g]Department of Basic Biology, Faculty of Life Science, SOKENDAI (Graduate University for Advanced Studies), Okazaki, Aichi 444-8787, Japan

Edited by Melanie H. Cobb, University of Texas Southwestern Medical Center, Dallas, TX, and approved October 3, 2017 (received for review April 30, 2017)

Optogenetics is a powerful tool to precisely manipulate cell signaling in space and time. For example, protein activity can be regulated by several light-induced dimerization (LID) systems. Among them, the phytochrome B (PhyB)–phytochrome-interacting factor (PIF) system is the only available LID system controlled by red and far-red lights. However, the PhyB–PIF system requires phycocyanobilin (PCB) or phytochromobilin as a chromophore, which must be artificially added to mammalian cells. Here, we report an expression vector that coexpresses HO1 and PcyA with Ferredoxin and Ferredoxin-NADP+ reductase for the efficient synthesis of PCB in the mitochondria of mammalian cells. An even higher intracellular PCB concentration was achieved by the depletion of biliverdin reductase A, which degrades PCB. The PCB synthesis and PhyB–PIF systems allowed us to optogenetically regulate intracellular signaling without any external supply of chromophores. Thus, we have provided a practical method for developing a fully genetically encoded PhyB–PIF system, which paves the way for its application to a living animal.

optogenetics | cell signaling | phytochrome | FRET | ERK

Intracellular signal transduction pathways are information-processing systems in which the information of input signals is processed and subsequently leads to the generation of output responses as cellular phenotypes (1, 2). These pathways are comprised of a series of biochemical reactions with cross-talk regulations and feedback regulations that form a highly complex network (3–5). While the complexity of the intracellular signaling network poses a significant challenge, considerable evidence has accumulated that certain network modules such as feedback loops have developed an intrinsic resistance to molecular targeted drugs (6–8), highlighting the critical importance of understanding the signaling network as a system.

Methods capable of rapidly and reversibly perturbing cellular systems are essential for analyzing the dynamics of feedback and cross-talk regulations. The perturbations have to be faster than the representative time constant of a feedback regulation to track the transient change in the system (9). While a chemical-induced dimerization (CID) system has been widely used to quickly perturb cellular signaling by small compounds (10), most CID systems are irreversible, and it is difficult to manipulate the dimerization at the subcellular level. Currently, several light-induced dimerization (LID) systems, in which photoactivatable proteins are dimerized by light in a reversible manner, are available. Among them, the cryptochrome 2 (CRY2) and cryptochrome-interacting basic helix–loop–helix1 (CIB1) pair has been widely used to control cell signaling through its light-induced heterodimerization (11–13). CRY2 associates with its binding partner CIB1 upon exposure to blue light within a few seconds, and the complex is dissociated under a dark condition within several minutes (14). The CRY2 protein utilizes flavin as a chromophore, and the CRY2–CIB1 LID system is thereby fully genetically encoded, so that it is not necessary to add a cofactor to mammalian cells. However, this system has potential drawbacks. First, the dissociation reaction has slow kinetics and is uncontrollable, though faster dissociation mutants of the CRY2–CIB1 pair have been reported recently (15). Second, the use of blue light for photoactivation of the CRY2–CIB1 is not compatible with fluorescence imaging with GFP-based biosensors such as FRET biosensors (16, 17).

Currently, phytochrome B (PhyB)–phytochrome-interacting factor (PIF) is the only LID system that operates at long wavelength light (14, 18, 19). PhyB ligates phycocyanobilin (PCB) or phytochromobilin as a photoabsorbing chromophore (20). Upon red light exposure, PhyB binds to PIF within seconds, and the resulting PhyB–PIF complex dissociates within seconds upon far-red light exposure. Taking advantage of its potential for quick and reversible control of association and dissociation by light, researchers have used the PhyB–PIF system to manipulate cellular signaling at higher resolution in both space and time (14, 18, 21). However, there is also a key disadvantage of the PhyB–PIF system. Namely, the chromophore is produced only in photosynthetic organisms; in other organisms, the chromophore must be added before the PhyB–PIF system can be applied. To overcome this issue, a PCB biosynthesis system has been constructed in bacterial and mammalian cells by expressing two biosynthetic enzymes, heme oxygenase1 (HO1) and PCB:ferredoxin (Fd) oxidoreductase (PcyA) (22–24) (Fig. 1*A*). So far, however, no PCB biosynthesis system has been used successfully to operate the PhyB–PIF system in mammalian cells, probably

Significance

Optical control of cell signaling has attracted much attention in recent years. Most optogenetic systems exploit blue light, as do fluorescent indicators such as FRET-based biosensors. Phytochrome B (PhyB)–phytochrome-interacting factor (PIF) is a red/far-red light-switchable heterodimerization system. However, PhyB requires phytochromobilin or phycocyanobilin (PCB) as a chromophore, which must be externally added to mammalian cells. To overcome this difficulty, we developed a system for an efficient synthesis of PCB in mammalian cells. Eventually, we found that PCB was synthesized by introducing all *PcyA*, *HO1*, *Fd*, and *Fnr* genes. The knockout or knockdown of biliverdin reductase A further enhanced PCB synthesis. This genetically encoded PCB synthesis system allowed us to manipulate cell signaling by red/far-red light without exogenous PCB addition.

Author contributions: Y.U., T.K., M.M., and K.A. designed research; Y.U., Y.G., S.O., and K.A. performed research; Y.U., Y.G., S.O., and K.A. analyzed data; and Y.U., M.M., and K.A. wrote the paper.

The authors declare no conflict of interest.

This article is a PNAS Direct Submission.

[1]To whom correspondence should be addressed. Email: k-aoki@nibb.ac.jp.

This article contains supporting information online at www.pnas.org/lookup/suppl/doi:10.1073/pnas.1707190114/-/DCSupplemental.

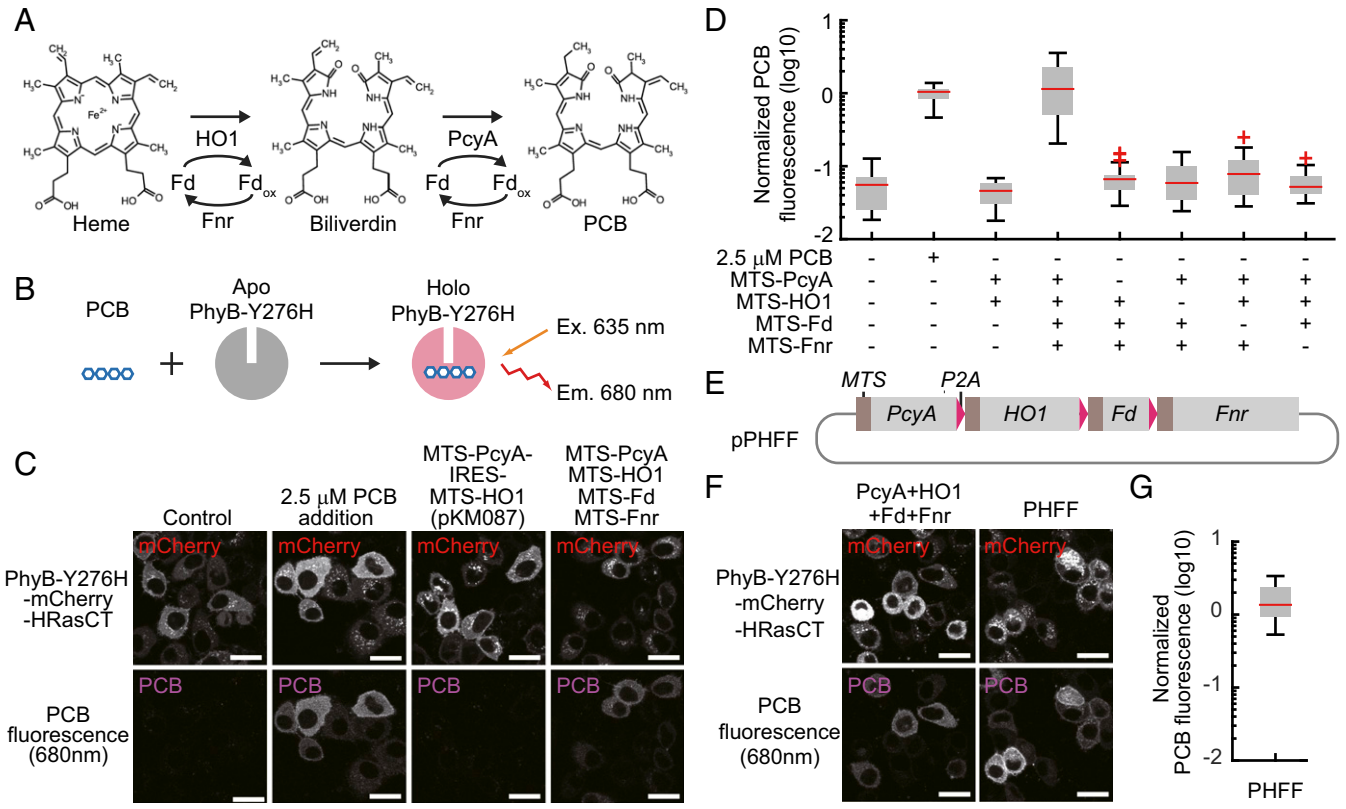

Fig. 1. PCB synthesis in mammalian cells. (*A*) The pathway of PCB synthesis in cyanobacteria. (*B*) Scheme for measurement of PCB fluorescence. The PhyB mutant PhyB-Y276H emits fluorescence from PCB when it binds to PCB. (*C*) Fluorescence images of PhyB-Y276H-mCherry-HRas C terminus (HRasCT) (*Upper*) and PCB fluorescence bound to PhyB-Y276H (*Lower*) are shown for the indicated condition in HeLa cells. pKM087 is a bicistronic vector expressing MTS-PcyA and MTS-HO1 (24). (Scale bars, 25 μm.) (*D*) Quantification of PCB synthesis. PCB fluorescence bound to PhyB-Y276H was divided by mCherry fluorescence, followed by normalization to the average PCB-bound PhyB-Y276H/mCherry value of 2.5 μM PCB-treated cells. The box extends from the first to the third quartile, with the whiskers denoting 1.5 times the interquartile range. Red crosses are outliers. $n = 24$. (*E*) Structure of the pPHFF plasmid expressing MTS-PcyA, MTS-HO1, MTS-Fd, and MTS-Fnr. These cDNAs are connected by the cDNAs of a self-cleaving 2A peptide, P2A, which allows stoichiometric expression of multiple proteins flanking the 2A peptide. (*F*) Fluorescence images of PhyB-Y276H-mCherry-HRasCT (*Upper*) and PCB (*Lower*) are shown as in *D*. (Scale bars, 20 μm.) (*G*) PCB fluorescence in HeLa cells expressing PHFF was quantified as in *D*. $n = 23$.

because the biosynthesis systems tested did not yield sufficient amounts of PCB for the PhyB–PIF system (Fig. 1*A*).

In this study, we demonstrate that PCB biosynthesis in mammalian cells is enormously boosted by the coexpression of *Fd* and *Fd-NADP*$^+$ reductase (*Fnr*) with *HO1* and *PcyA*. A further increase in PCB synthesis is achieved by knockout (KO) or knockdown (KD) of biliverdin reductase A (*BVRA*). Using this genetically encoded PCB synthesis system, we have succeeded in optogenetic control of cell signaling by the PhyB–PIF system in the absence of exogenous chromophores.

Results

Reconstitution of the PCB Synthesis Pathway in Mammalian Cells. Two enzymes, heme oxygenase (25) and ferredoxin-dependent bilin reductase (26, 27), are committed to phytochrome chromophore biosynthesis from heme. In photosynthetic organisms such as cyanobacteria, PCB is produced from heme through HO1-mediated degradation, followed by PcyA-mediated biliverdin reduction (Fig. 1*A*). Both reactions are coupled with a reduction by reduced Fd. The oxidized Fd (Fd$_{ox}$) is then recycled by Fnr to regenerate reduced Fd. In our preliminary experiments, expression of HO1 and PcyA derived from *Thermosynechococcus elongatus* BP-1 was not sufficient for operation of the PhyB–PIF system in mammalian cells. We hypothesized that the failure might have been due to the lack of Fd and Fnr. Because heme exists primarily at mitochondria in mammalian cells (28, 29), we attempted to coexpress Fd and Fnr derived from *Synechocystis* sp. PCC6803 with HO1 and PcyA to reconstitute the PCB synthetic pathway in human cells.

To quantify the amount of PCB in a living cell, we employed the Tyr-276–His mutant of PhyB (PhyB-Y276H), which emits red fluorescence upon binding to PCB (30) (Fig. 1*B*). The PhyB-Y276H protein was fused with mCherry, which was used as an internal standard, and the H-Ras C terminus (HRasCT) was used for plasma membrane localization. HeLa cells expressing PhyB-Y276H-mCherry-HRasCT emanated 680 nm red fluorescence in the presence of exogenous PCB (Fig. 1*C*). Müller et al. (24) realized PCB synthesis in mammalian cells by using a pKM087 expression vector that encodes mitochondria-targeting sequence (MTS) fused with PcyA and MTS-HO1. However, the fluorescence from PhyB-Y276H was below the detectable level in pKM087-expressing HeLa cells (Fig. 1 *C* and *D*).

To our surprise, when MTS-Fd and MTS-Fnr were coexpressed with MTS-PcyA and MTS-HO1, the red fluorescence of PhyB-Y276H from HeLa cells became almost comparable to that observed in the presence of 2.5 μM PCB (Fig. 1 *C* and *D*). Exclusion of any one of these four genes abolished the fluorescence from the cells (Fig. 1*D*). Human homolog of HO1, Fd, or Fnr was unable to substitute for HO1, Fd, or Fnr in PCB synthesis (Fig. S1). These data indicated that PcyA, HO1, Fd, and Fnr, which are derived from *T. elongatus* BP-1 or *Synechocystis* sp. PCC6803, were required for the efficient PCB production in mammalian cells.

To facilitate gene delivery, these four genes were connected with the cDNA of the self-cleaved P2A peptide, generating a synthetic gene "PHFF" (Fig. 1*E* and Fig. S2). The HeLa cells transfected with the pPHFF expression vector for PHFF emanated red fluorescence from PhyB-Y276H at a level comparable to that of cells expressing the four genes independently (Fig. 1 *F* and *G*). PCB is known to be covalently attached to PhyB. The covalent attachment of PCB to the PhyB was confirmed by SDS PAGE followed by zinc blot analysis (Fig. S3). Moreover, PHFF-expressing *Schizosaccharomyces pombe* produced intracellular PCB to the level evoked by the addition of a saturating amount of extracellular PCB (Fig. S4 and Table S1).

LID by the PHFF–PhyB–PIF System. Next, we examined whether expression of pPHFF is sufficient for PhyB binding to PIF. For this purpose, PhyB-mCherry-HRasCT and PIF-mEGFP were coexpressed at the plasma membrane and cytosol, respectively, with pPHFF. The cells were reciprocally illuminated with red and far-red lights to turn on and off, respectively, the binding of PIF-mEGFP to PhyB-mCherry-HRasCT at the plasma membrane (Fig. 2*A*). We examined four pairs of PhyB and PIF—that is, PhyB (1–908 aa) and PhyB621 (1–621 aa) for the PhyBs (Fig. 2*B*), and PIF3 and PIF6 for the PIFs (31). PhyB621 was comprised of the minimal photosensory core—namely, the PAS-like, GAF, and Phy domains (20). The pair of PhyB and PIF3 resulted in a clear change in PIF3 distribution upon red and far-red light exposure, whereas the pair of PhyB621 and PIF3 showed a limited subcellular relocalization (Fig. 2 *C* and *D*, *Upper* and Movie S1). PIF6 was also associated with PhyB and PhyB621 under the red light exposure, while it was not completely dissociated from PhyB and PhyB621 by the far-red light (Fig. 2 *C* and *D*, *Lower* and Movie S1). The reductions of cytoplasmic PIF-mEGFP intensities compared with the far-red light condition were quantified for each of these four combinations (Fig. 2 *D*–*G*), indicating fast and reversible membrane translocation of PIF by red and far-red light exposure on the second time scale (Fig. 2 *D*–*G*). Interestingly, PIF3 reproducibly showed faster association and dissociation rate constants than PIF6.

Enhancement of PhyB–PIF LID by the Depletion of BVRA. To further enhance PhyB–PIF LID, we depleted BVRA, which metabolizes biliverdin and PCB into bilirubin and phycocyanorubin, respectively (32) (Fig. 3*A*). To this end, we established *BVRA* KO HeLa cells by using the CRISPR/Cas9 system. As expected, the KO of *BVRA* reduced intracellular bilirubin, as visualized by UnaG, a bilirubin sensor (33) (Fig. S5). In *BVRA* KO HeLa cells, PhyB-Y276H fluorescence was increased to approximately threefold the level in control HeLa cells (Fig. 3 *B* and *C*). RNAi-mediated KD of *BVRA* also increased PhyB-Y276H fluorescence (Fig. S6). The enhancement of PhyB-Y276H fluorescence may

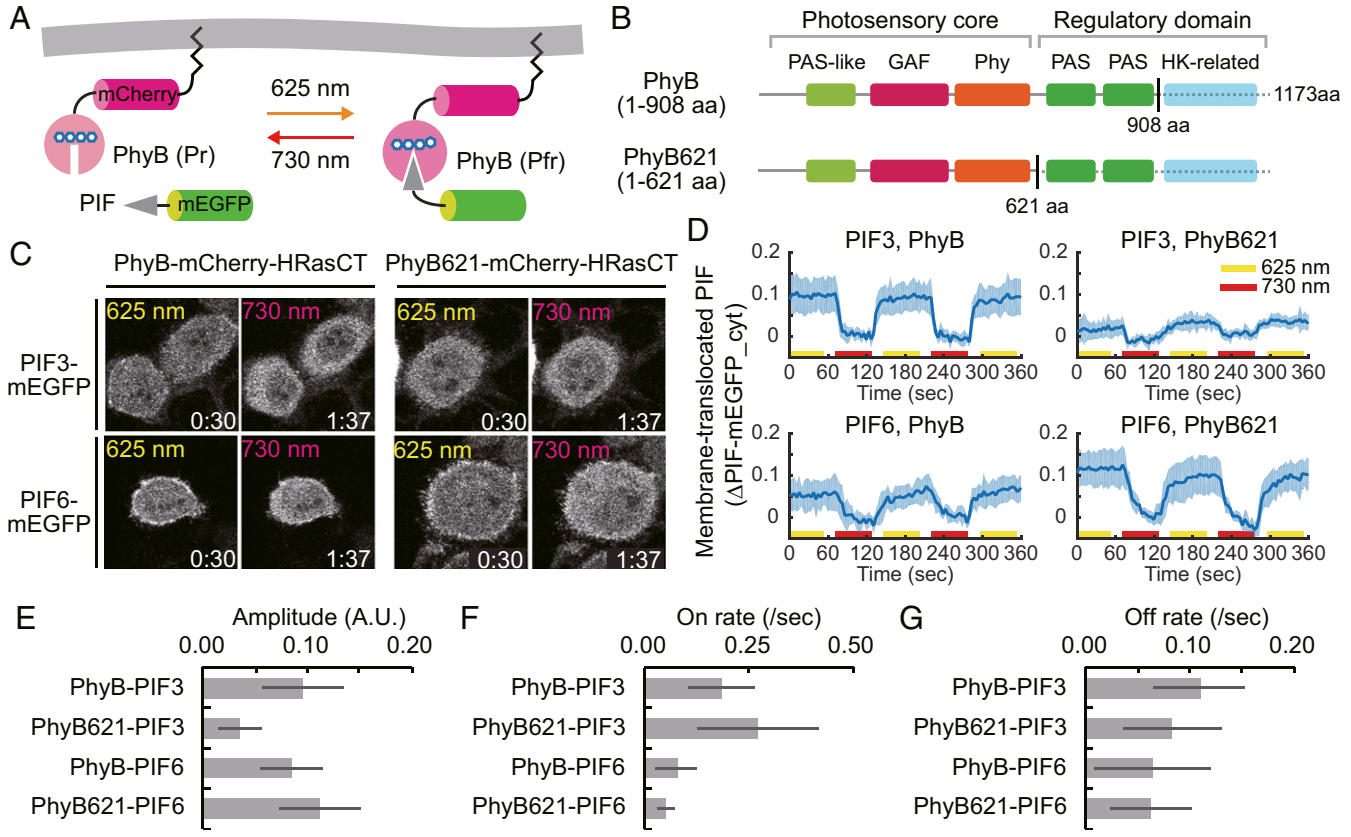

Fig. 2. PhyB–PI LID with endogenously-synthesized PCB. (*A*) A schematic representation of the PhyB–PIF LID system. PhyB-mCherry-HRasCT is localized at the plasma membrane. PIF fused with mEGFP is translocated to the plasma membrane through the binding to PhyB-mCherry-HRasCT upon illumination with red light (625 nm). Illumination with far-red light (730 nm) induces dissociation of the PhyB–PIF heterodimer. (*B*) Domain structures of PhyB (1–908 aa) and PhyB621 (1–621 aa). (*C*) PhyB–PIF LID assay. PIF-mEGFP fluorescence images are shown in HeLa cells expressing PHFF, PhyB-mCherry-HRasCT (*Left* column) or PhyB621-mCherry-HRasCT (*Right* column) and PIF3-mEGFP (*Upper*) or PIF6-mEGFP (*Lower*) upon the illumination with red light (*Left*) and far-red light (*Right*). (*D*) Membrane-recruited PIF-mEGFP was quantified by the fractional change in the fluorescence intensity of PIF-mEGFP at the cytoplasm in comparison with that under the condition of far-red light exposure. The average values (bold lines) are plotted as a function of time with the SD. $n = 8$. (*E*–*G*) Quantification of PhyB–PIF LID. Amplitude (*E*), on rate (*F*), and off rate (*G*) of PIF membrane translocation were quantified by curve fitting the data in *D* with a single exponential curve. The bar graphs show the average values with the SD. A.U., arbitrary unit.

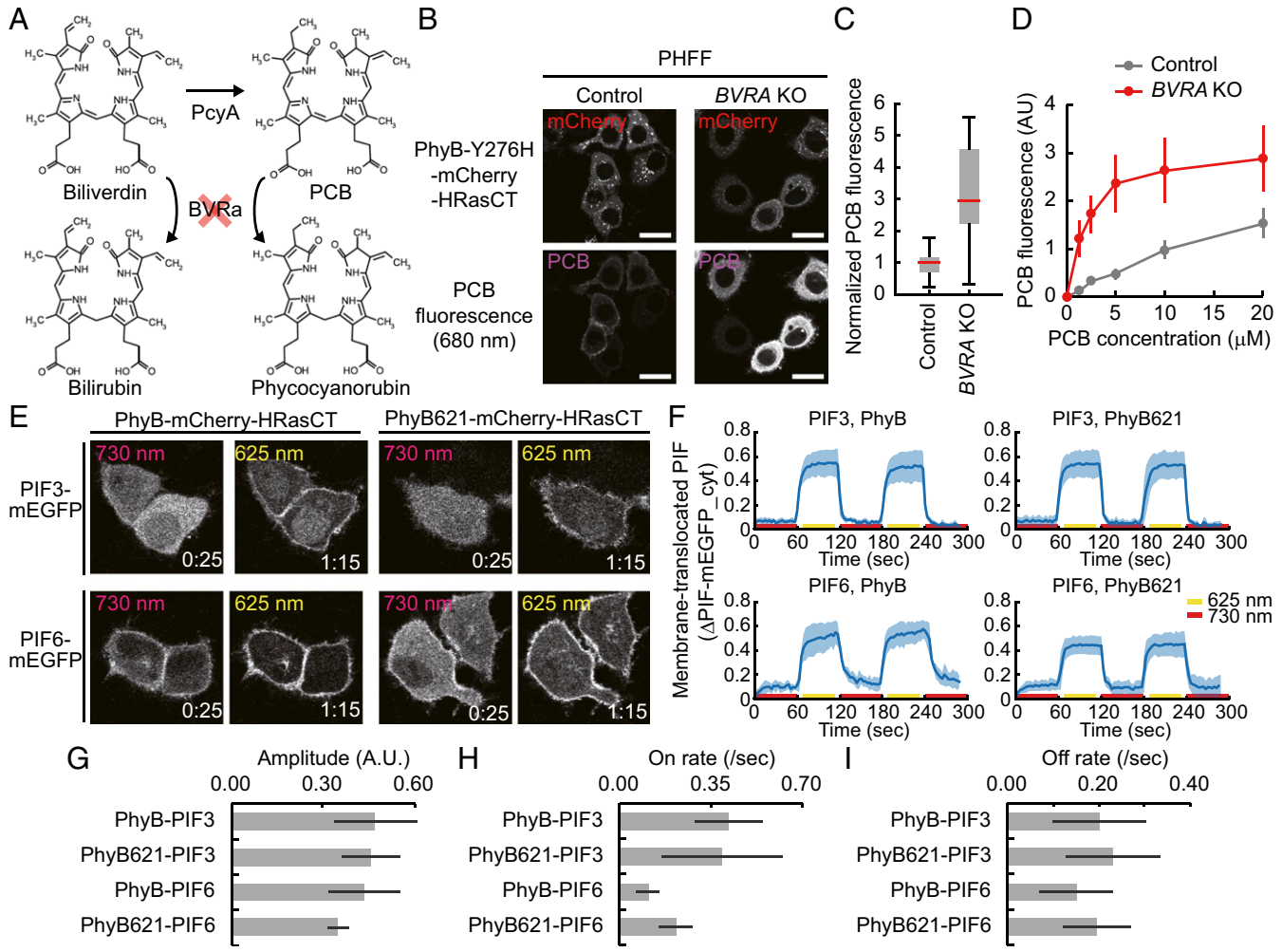

Fig. 3. Enhancement of PCB synthesis by KO of the *BVRA* gene. (*A*) Scheme of the metabolic pathway of biliverdin and PCB. BVRA degrades both biliverdin and PCB, generating bilirubin and phycocyanorubin, respectively. (*B*) PCB synthesis in control (*Left*) and *BVRA* KO HeLa cells (*Right*). Representative images of PhyBY276H-mCherry-HRas CT (*Upper*) and PCB (*Lower*) are shown as in Fig. 1*C*. (Scale bars, 25 μm.) (*C*) PCB fluorescence in the control and BVRA KO cells was divided by mCherry fluorescence and normalized to the average PCB/mCherry value in control cells as 1.0. The normalized PCB fluorescence is shown as a box plot as in Fig. 1*D*. (*D*) Purified PCB was supplied to control (gray) and *BVRA* KO (red) HeLa cells expressing PhyBY276H-mCherry-HRasCT. PCB fluorescence is plotted as a function of PCB concentration. (*E*) PhyB–PIF LID assay. PIF-mEGFP fluorescence images are shown in *BVRA* KO HeLa cells as in Fig. 2*C*. (*F*) Quantification of PhyB–PIF LID. Membrane-recruited PIF-mEGFP was quantified, and the average values (bold lines) are plotted as in Fig. 2*D*. $n = 8$. (*G–I*) Quantification of PhyB–PIF LID. Amplitude (*G*), on rate (*H*), and off rate (*I*) of PIF membrane translocation were quantified by curve fitting the data in *F* with a single exponential curve. The bar graphs show the average values with the SD. A.U., arbitrary unit.

have been due to the decrease in degradation of PCB, because *BVRA* KO HeLa cells demonstrated higher PCB fluorescence by the addition of purified PCB than control HeLa cells did (Fig. 3*D*). Meanwhile, it is reported that supplementation of Heme precursor, 5-aminolevulinic acid (ALA), and iron(ii) sulfate increases Biliverdin biosynthesis up to threefold (34). Contrary to our expectation, these treatments did not significantly increase PCB synthesis in either control HeLa or BVRA KO HeLa cells that expressed PHFF (Fig. S7). Notably, neither the expression of PHFF nor the depletion of BVRA affected cell growth rates in HeLa cells and mouse embryonic stem cells (mESCs) (Fig. S8).

Next, we evaluated the effect of *BVRA* KO on LID in the same PhyB and PIF pairs as in Fig. 2*E*. In *BVRA* KO HeLa cells expressing PHFF, both the PIF3 and PhyB pair and PIF3 and PhyB621 pair showed distinct translocation of PIF3-mEGFP upon red light and far-red light exposure (Fig. 3*E*, *Upper* and Movie S2). PIF6 also demonstrated clear association with PhyB and PhyB621 by red-light exposure, but a substantial amount of PIF6-mEGFP remained at the plasma membrane even under a far-red light condition in both the combinations with PhyB and that with PhyB621 in *BVRA* KO HeLa cells (Fig. 3*E*, *Lower* and Movie S2). The quantification showed a much better response of PIF-mEGFP translocation in *BVRA* KO cells (Fig. 3 *F–I*) than control cells (Fig. 2*D*) under all conditions. The PIF3 and PhyB pair exhibited rapid translocation almost comparable to that of the PIF3 and PhyB621 pair, with reversible PIF translocation (Fig. 3 *F–I*, *Upper*). Meanwhile, slower and smaller translocations of PIF6-mEGFP were observed with the PIF6 and PhyB pair and PIF6 and PhyB621 pair, respectively (Fig. 3 *F–I*, *Lower*). On the other hand, we verified whether the PhyB–PIF3 combination is effective in other types of cells. PCB synthesis was also observed in mESCs and mouse embryonic fibroblasts (MEFs) that expressed PHFF and shRNA against mouse *BVRA* (m*BVRA*) (Figs. S6 and S9). Under this condition, PhyB–PIF3 LID was reproducibly observed in mESCs (Fig. S9).

Application of the PhyB–PIF System to Manipulating Signal Transduction. Finally, we employed the genetically encoded PhyB–PIF system to control intracellular signaling. It is known that activation of Rac1, a

small GTPase, leads to actin reorganization and lamellipodia formation (35). To optogenetically activate the endogenous Rac1 protein Tiam1, a Rac1-specific guanine nucleotide exchange factor (36) was fused with PIF3 and mEGFP, and this chimeric protein was recruited to the plasma membrane through binding to PhyB-mCherry-HRasCT upon exposure to red light (Fig. 4*A*). Indeed, red light exposure induced rapid formation of thin lamellipodia along the cell periphery in HEK-293 cells expressing sh-hBVRA (Fig. 4 *B* and *C* and Movie S3), indicating the activation of Rac1 by light illumination.

One advantage of the PhyB–PIF system is that it enables both the manipulation of cell signaling and detection of the output signals with a GFP reporter or CFP/YFP-based FRET biosensor. The ERK MAP kinase pathway was activated by the recruitment of CRaf-PIF3 to the plasma membrane by red light, and the subsequent activation of ERK was monitored by EKAREV-NLS, an ERK FRET biosensor (37) (Fig. 4*D*). Importantly, the excitation light for the FRET biosensor caused slight PhyB activation, and therefore, the nonspecific activation was prevented by global illumination with far-red light. The FRET/CFP ratio, which correlated with ERK activity (11), was increased upon red light illumination (Fig. 4*E* and Movie S4), and this increase was suppressed by far-red light illumination (Fig. 4*F*).

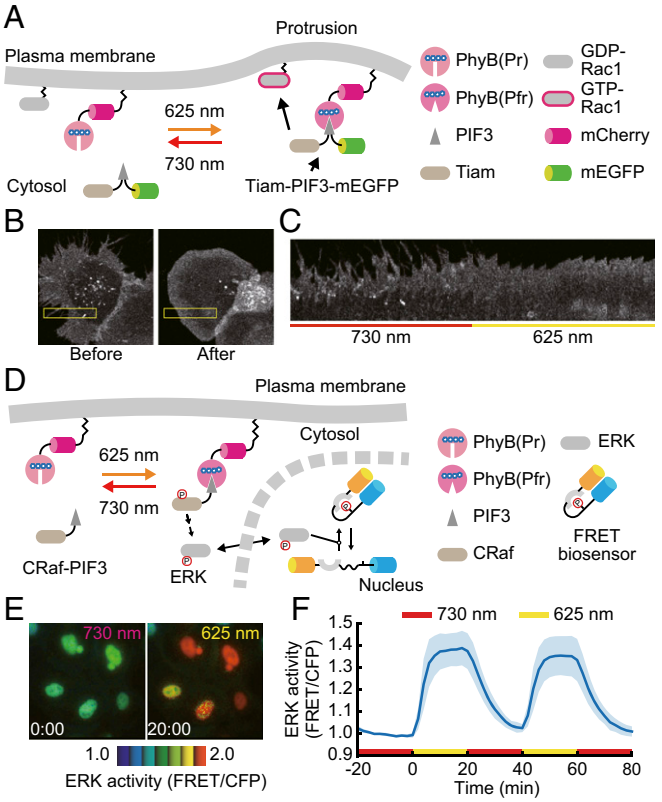

Fig. 4. Manipulation of intracellular signaling by the PhyB–PIF system with endogenously synthesized PCB. (*A*) Schematic representation of Rac1 activation by the PhyB–PIF system. Tiam1-PIF3-mEGFP, a Rac1 activator, is translocated to the plasma membrane upon exposure to red light, leading to Rac1 activation. (*B* and *C*) *BVRA* KD HEK-293 cells stably expressing PhyB-mCherry-HRasCT and Tiam1-PIF3-mEGFP were transfected with pPHFF. Two days after transfection, the cells were subjected to a far-red light condition (before), followed by a red light condition (after). Fluorescence images of PhyB-mCherry-HRasCT (*B*) and the montage image in the yellow box of *B* (*C*) are shown. (Magnification: *B*, 60×.) (*D*) Schematic representation of ERK activation by the PhyB–PIF system. Recruitment of CRaf-PIF3 to the membrane by PhyB–PIF LID results in ERK activation, which is monitored by a FRET biosensor, EKAREV-NLS. (*E* and *F*) *BVRA* KO HeLa cells expressing PHFF, PhyB-mCherry-HRasCT, CRaf-PIF3, and EKAREV-NLS were imaged under the conditions of far-red light and red light illumination. Images of ERK activity are represented in the IMD mode (*E*). The average ERK activity (normalized FRET/CFP ratio) was quantified and plotted as a function of time with the SD (*F*). $n = 9$.

Discussion

We induced PCB synthesis in mammalian cells through the expression of a synthetic gene, PHFF, that was made up of the four genes *PcyA*, *HO1*, *Fd*, and *Fnr*, which are derived from *T. elongatus* BP-1 or *Synechocystis* sp. PCC6803. Moreover, *BVRA* KO or *BVRA* KD was shown to increase the level of cellular PCB by reducing the metabolism of biliverdin and PCB (32). The amount of synthesized PCB was sufficient for use in a genetically encoded PhyB–PIF system for the modulation of intracellular signaling.

Müller et al. (24) have reported PCB synthesis by the expression of *HO1* and *PcyA* in mammalian cells, but we found that the amount of PCB synthesized by this method was not sufficient for operation of the PhyB–PIF system. Of note, mammalian cells endogenously express Fd-1, an Fd-like protein (also known as adrenodoxin) (38). However, the amino acid sequence homology between human Fd-1 and *Synechocystis* sp. PCC 6803 Fd was limited to 26%. Additionally, sequence and structure studies of mammalian Fnr/adrenodoxin reductase suggested no functional overlap with *Synechocystis* sp. PCC 6803 Fnr (39, 40). The robust increase in PhyB-Y276H fluorescence observed in the present study (Fig. 1 *C* and *D*) strongly suggests that mammalian ferrodoxin-1/adrenodixin and Fnr/adrenodoxin reductase cannot support the PCB synthesis by cyanobacterial *HO1* and *PcyA*.

Faster association and dissociation kinetics were observed in the PIF3–PhyB bindings in comparison with the PIF6–PhyB bindings (Figs. 2 and 3). PIF6 was originally reported to show fast and reversible bindings to PhyB in the LID system (18). However, under our experimental conditions, PIF6 tended to be retained at the plasma membrane even after far-red light exposure (Figs. 2 and 3). Although the precise mechanisms underlying this retention are still unclear, the sustained binding of PIF6 to PhyB may leak signals of the LID system even under far-red light illumination and eventually decrease ON and OFF responses. For this reason, PIF3 would be more suitable than PIF6 as a binding partner of PhyB in the PhyB–PIF system.

Depletion of BVRA by CRISPR/Cas9-mediated gene KO or shRNA resulted in an enhancement of PCB synthesis and thereby an increase in the efficiency of PhyB–PIF LID (Fig. 3 and Fig. S6). Heme and its metabolites, biliverdin and bilirubin, are known to have diverse physiological functions including electron transfer and antioxidant and cell signaling, respectively (28, 41, 42), though their cellular functions remain controversial (43). In our experiments, we did not observe any detectable effects of PHFF expression and/or *BVRA* KD on cell growth rates in HeLa cells and mESCs (Fig. S8). This might be because biliverdin and bilirubin are delivered from the serum. Additionally, it should be noted the possible alteration of insulin signaling by depletion of the *BVRA* gene (44). Therefore, new strategies are needed to improve PCB synthesis without affecting BVRA function.

The genetically encoded system of PCB synthesis will provide a potential advantage for establishing transgenic animals that stably synthesize PCB endogenously, thereby enabling the optogenetic manipulation of cell signaling in deeper tissues without injecting PCB. Biliverdin-bound PhyB mutants or other phytochromes should also be explored in future studies.

Materials and Methods

pKM087 was the kind gift of Dr. Weber (University of Freiburg, Freiburg, Germany) (24). The cDNAs of *PcyA* and *HO1*, which were originally derived from *T. elongatus* BP-1, were amplified from pKM087. The cDNAs of *Fd* and *Fnr* of *Synechocystis* sp. PCC 6803 were synthesized with codon optimization

for humans by GenScript. The MTS (MSVLTPLLLRGLTGSARRLP) was derived from human cytochrome C oxidase subunit VIII. These cDNAs were subcloned into the pCAGGS vector (45) to generate pCAGGS-MTS-PcyA, pCAGGS-MTS-PcyA-mCherry, pCAGGS-MTS-HO1-mCFP, pCAGGS-MTS-Fd-mVenus, and pCAGGS-MTS-Fnr-tagBFP. The cDNA of PHFF, which contained MTS-PcyA-FLAG-P2A-MTS-HA-HO1-P2A-MTS-Myc-Fd-P2A-MTS-Fnr-T7, was synthesized by GenScript and subcloned into the pCAGGS vector to obtain pPHFF. The cDNA sequence of PHFF is included in Fig. S2. pcDNA3.1-UnaG-mCherry was a kind gift from Atsushi Miyawaki (RIKEN, Wako, Japan) (33). The details of other materials and methods are described in *SI Materials and Methods*.

ACKNOWLEDGMENTS. We thank W. Weber (pKM087), A. Bradley (PiggyBac), F. Zhang (pX459 and lentiCRISPR v2), H. Miyoshi (pCMV-VSV-G-RSV-Rev), Didier Trono (psPax2), and A. Miyawaki (pcDNA3.1-UnaG-mcherry) for the plasmids; T. Fujimori for mESCs and MEFs; J. Nakayama for WT fission yeasts; A. Kawagishi, K. Hirano, N. Nishimoto, K. Onoda, and E. Ebine for their technical assistance; and members of the M.M. laboratory and the K.A. laboratory for their helpful input. S.O., M.M., and K.A. were supported by the Platform for Dynamic Approaches to Living System from the Ministry of Education, Culture, Sports, and Science, Japan, and Core Research for Evolutional Science and Technology, Japan Science and Technology Agency. K.A. was supported by Japan Society for the Promotion of Science KAKENHI Grants 16H01425, 16H01447, and 16KT0069; the Hori Sciences and Arts Foundation; Takeda Science Foundation; and the Nakajima Foundation.

1. Kholodenko B, Yaffe MB, Kolch W (2012) Computational approaches for analyzing information flow in biological networks. *Sci Signal* 5:re1.
2. Kholodenko BN (2006) Cell-signalling dynamics in time and space. *Nat Rev Mol Cell Biol* 7:165–176.
3. Mendoza MC, Er EE, Blenis J (2011) The Ras-ERK and PI3K-mTOR pathways: Cross-talk and compensation. *Trends Biochem Sci* 36:320–328.
4. Lemmon MA, Schlessinger J (2010) Cell signaling by receptor tyrosine kinases. *Cell* 141:1117–1134.
5. Oda K, Matsuoka Y, Funahashi A, Kitano H (2005) A comprehensive pathway map of epidermal growth factor receptor signaling. *Mol Syst Biol* 1:2005.0010.
6. Fujita Y, Komatsu N, Matsuda M, Aoki K (2014) Fluorescence resonance energy transfer based quantitative analysis of feedforward and feedback loops in epidermal growth factor receptor signaling and the sensitivity to molecular targeting drugs. *FEBS J* 281:3177–3192.
7. Prahallad A, et al. (2012) Unresponsiveness of colon cancer to BRAF(V600E) inhibition through feedback activation of EGFR. *Nature* 483:100–103.
8. Friday BB, et al. (2008) BRAF V600E disrupts AZD6244-induced abrogation of negative feedback pathways between extracellular signal-regulated kinase and Raf proteins. *Cancer Res* 68:6145–6153.
9. Inoue T, Meyer T (2008) Synthetic activation of endogenous PI3K and Rac identifies an AND-gate switch for cell polarization and migration. *PLoS One* 3:e3068.
10. DeRose R, Miyamoto T, Inoue T (2013) Manipulating signaling at will: Chemically-inducible dimerization (CID) techniques resolve problems in cell biology. *Pflugers Arch* 465:409–417.
11. Aoki K, et al. (2013) Stochastic ERK activation induced by noise and cell-to-cell propagation regulates cell density-dependent proliferation. *Mol Cell* 52:529–540.
12. Kennedy MJ, et al. (2010) Rapid blue-light-mediated induction of protein interactions in living cells. *Nat Methods* 7:973–975.
13. Zhang K, Cui B (2015) Optogenetic control of intracellular signaling pathways. *Trends Biotechnol* 33:92–100.
14. Tischer D, Weiner OD (2014) Illuminating cell signalling with optogenetic tools. *Nat Rev Mol Cell Biol* 15:551–558.
15. Taslimi A, et al. (2016) Optimized second-generation CRY2-CIB dimerizers and photoactivatable Cre recombinase. *Nat Chem Biol* 12:425–430.
16. Kiyokawa E, Hara S, Nakamura T, Matsuda M (2006) Fluorescence (Förster) resonance energy transfer imaging of oncogene activity in living cells. *Cancer Sci* 97:8–15.
17. Endo M, Ozawa T (2017) Strategies for development of optogenetic systems and their applications. *J Photochem Photobiol C Photochem Rev* 30:10–23.
18. Levskaya A, Weiner OD, Lim WA, Voigt CA (2009) Spatiotemporal control of cell signalling using a light-switchable protein interaction. *Nature* 461:997–1001.
19. Shimizu-Sato S, Huq E, Tepperman JM, Quail PH (2002) A light-switchable gene promoter system. *Nat Biotechnol* 20:1041–1044.
20. Anders K, Essen LO (2015) The family of phytochrome-like photoreceptors: Diverse, complex and multi-colored, but very useful. *Curr Opin Struct Biol* 35:7–16.
21. Toettcher JE, Weiner OD, Lim WA (2013) Using optogenetics to interrogate the dynamic control of signal transmission by the Ras/Erk module. *Cell* 155:1422–1434.
22. Gambetta GA, Lagarias JC (2001) Genetic engineering of phytochrome biosynthesis in bacteria. *Proc Natl Acad Sci USA* 98:10566–10571.
23. Mukougawa K, Kanamoto H, Kobayashi T, Yokota A, Kohchi T (2006) Metabolic engineering to produce phytochromes with phytochromobilin, phycocyanobilin, or phycoerythrobilin chromophore in Escherichia coli. *FEBS Lett* 580:1333–1338.
24. Müller K, et al. (2013) Synthesis of phycocyanobilin in mammalian cells. *Chem Commun (Camb)* 49:8970–8972.
25. Muramoto T, Kohchi T, Yokota A, Hwang I, Goodman HM (1999) The Arabidopsis photomorphogenic mutant hy1 is deficient in phytochrome chromophore biosynthesis as a result of a mutation in a plastid heme oxygenase. *Plant Cell* 11:335–348.
26. Kohchi T, et al. (2001) The Arabidopsis HY2 gene encodes phytochromobilin synthase, a ferredoxin-dependent biliverdin reductase. *Plant Cell* 13:425–436.
27. Frankenberg N, Mukougawa K, Kohchi T, Lagarias JC (2001) Functional genomic analysis of the HY2 family of ferredoxin-dependent bilin reductases from oxygenic photosynthetic organisms. *Plant Cell* 13:965–978.
28. Ponka P (1999) Cell biology of heme. *Am J Med Sci* 318:241–256.
29. Ajioka RS, Phillips JD, Kushner JP (2006) Biosynthesis of heme in mammals. *Biochim Biophys Acta Mol Cell Res* 1763:723–736.
30. Fischer AJ, et al. (2005) Multiple roles of a conserved GAF domain tyrosine residue in cyanobacterial and plant phytochromes. *Biochemistry* 44:15203–15215.
31. Khanna R, et al. (2004) A novel molecular recognition motif necessary for targeting photoactivated phytochrome signaling to specific basic helix-loop-helix transcription factors. *Plant Cell* 16:3033–3044.
32. Terry MJ, Maines MD, Lagarias JC (1993) Inactivation of phytochrome- and phycobiliprotein-chromophore precursors by rat liver biliverdin reductase. *J Biol Chem* 268:26099–26106.
33. Kumagai A, et al. (2013) A bilirubin-inducible fluorescent protein from eel muscle. *Cell* 153:1602–1611.
34. Rodriguez EA, et al. (2016) A far-red fluorescent protein evolved from a cyanobacterial phycobiliprotein. *Nat Methods* 13:763–769.
35. Kamai T, et al. (2003) Significant association of Rho/ROCK pathway with invasion and metastasis of bladder cancer. *Clin Cancer Res* 9:2632–2641.
36. Michiels F, et al. (1997) Regulated membrane localization of Tiam1, mediated by the NH2-terminal pleckstrin homology domain, is required for Rac-dependent membrane ruffling and C-Jun NH2-terminal kinase activation. *J Cell Biol* 137:387–398.
37. Komatsu N, et al. (2011) Development of an optimized backbone of FRET biosensors for kinases and GTPases. *Mol Biol Cell* 22:4647–4656.
38. Grinberg AV, et al. (2000) Adrenodoxin: Structure, stability, and electron transfer properties. *Proteins* 40:590–612.
39. Ziegler GA, Vonrhein C, Hanukoglu I, Schulz GE (1999) The structure of adrenodoxin reductase of mitochondrial P450 systems: Electron transfer for steroid biosynthesis. *J Mol Biol* 289:981–990.
40. Hanukoglu I, Gutfinger T (1989) cDNA sequence of adrenodoxin reductase. Identification of NADP-binding sites in oxidoreductases. *Eur J Biochem* 180:479–484.
41. Baranano DE, Rao M, Ferris CD, Snyder SH (2002) Biliverdin reductase: A major physiologic cytoprotectant. *Proc Natl Acad Sci USA* 99:16093–16098.
42. Lerner-Marmarosh N, Miralem T, Gibbs PEM, Maines MD (2008) Human biliverdin reductase is an ERK activator; hBVR is an ERK nuclear transporter and is required for MAPK signaling. *Proc Natl Acad Sci USA* 105:6870–6875.
43. Maghzal GJ, Leck MC, Collinson E, Li C, Stocker R (2009) Limited role for the bilirubin-biliverdin redox amplification cycle in the cellular antioxidant protection by biliverdin reductase. *J Biol Chem* 284:29251–29259.
44. Hinds TD, Jr, et al. (2016) Biliverdin reductase A attenuates hepatic steatosis by inhibition of glycogen synthase kinase (GSK) 3β phosphorylation of serine 73 of peroxisome proliferator-activated receptor (PPAR) α. *J Biol Chem* 291:25179–25191.
45. Niwa H, Yamamura K, Miyazaki J (1991) Efficient selection for high-expression transfectants with a novel eukaryotic vector. *Gene* 108:193–199.
46. Aoki K, Yamada M, Kunida K, Yasuda S, Matsuda M (2011) Processive phosphorylation of ERK MAP kinase in mammalian cells. *Proc Natl Acad Sci USA* 108:12675–12680.
47. Yusa K, Rad R, Takeda J, Bradley A (2009) Generation of transgene-free induced pluripotent mouse stem cells by the piggyBac transposon. *Nat Methods* 6:363–369.
48. Ran FA, et al. (2013) Genome engineering using the CRISPR-Cas9 system. *Nat Protoc* 8:2281–2308.
49. Gibson DG, et al. (2009) Enzymatic assembly of DNA molecules up to several hundred kilobases. *Nat Methods* 6:343–345.
50. Akagi T, Sasai K, Hanafusa H (2003) Refractory nature of normal human diploid fibroblasts with respect to oncogene-mediated transformation. *Proc Natl Acad Sci USA* 100:13567–13572.
51. Moreno S, Klar A, Nurse P (1991) Molecular genetic analysis of fission yeast Schizosaccharomyces pombe. *Methods Enzymol* 194:795–823.
52. Suga M, Hatakeyama T (2005) A rapid and simple procedure for high-efficiency lithium acetate transformation of cryopreserved Schizosaccharomyces pombe cells. *Yeast* 22:799–804.